Chapter 6
Masonry Stairways

Abstract. Statics of cantilevered masonry stairs, the so-called "*scale alla romana*", is the subject of this chapter. The flights of these stairs are cantilevered from a wall and connected by small vaults constituting the landings. The flight is composed of a long masonry vault having a depressed transverse sectional profile. For this type of structure, the existence of an admissible equilibrium may appear paradoxical. A new resistant model of these stairs is proposed in the context of the no tension models. The model is validated by numerical investigations and comparisons with tests.

6.1 Geometrical Features of Masonry Stairs: Cantilevered Stairs

There are many different types of masonry stairways. One very common type in Italy is the so-called "*scale alla romana*" (Roman stairs), whose flights are cantilevered from walls and connected by small vaults constituting the landings. In the following sections such an arrangement will be referred to as "*cantilevered stairways"*.

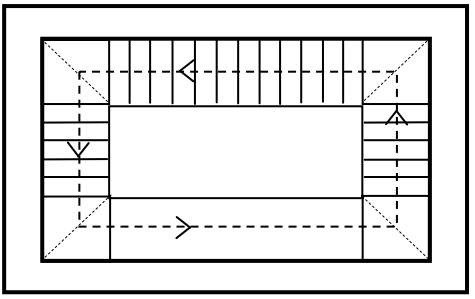

Fig. 6.1. Cantilevered stairway with open well and landings made up of quarter cloister vaults

M. Como: Statics of Historic Masonry Constructions, SSSSM 1, pp. 381–399.
springerlink.com

Figure 6.1 shows the plan of this type of stairs. Usually there are three straight flights winding around an open well, four intermediate landings, and a long floor-level landing, or stairhead, that provides access to the different quarters on each story. Figure 6.2 shows a view of the corner where the flight meets the landing composed of a quarter cloister vault.

Fig. 6.2. Stair corner at the flight-to-landing intersection

The structure of the flights is composed of a long masonry vault having a depressed transverse sectional profile. They are built with bricks or stones laid in different arrangements (Fig. 6.3).

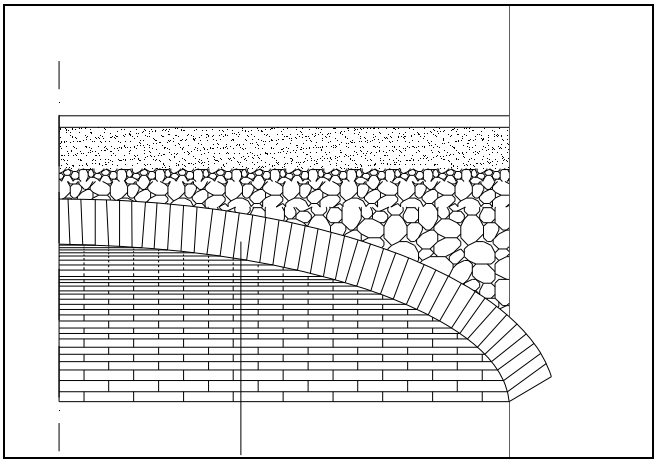

Fig. 6.3. Typical section of a cantilevered flight

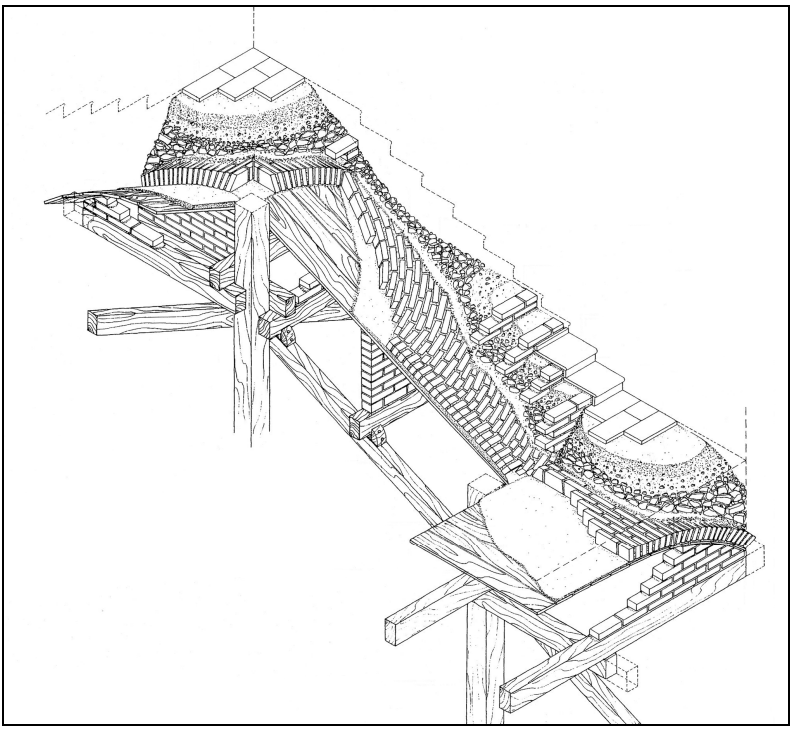

Fig. 6.4. Centering and scaffolding used to build cantilevered stairs (Giovanetti, 1997).

A thick layer of rubble and mortar is cast over the vaults, and the steps built on top of these bases (fig. 6.3 and 6.4).

6.2 Brick Layout

Figure 6.5 shows the typical brick pattern of a cantilevered stair with three flights and a long main landing. The stair angles around in the clockwise direction. Blocks – either stones or bricks – are laid along the axes of three-dimensional curves. The geometrical layout reveals the aim of the builder to keep the brick courses tight on the centering during construction.

Construction of a flight progresses bottom-up. The first course blocks are positioned parallel to the borders of the lower landing. Subsequent courses are then laid along arches in a gradual curve toward the well hole, i.e., toward the flight's inner sides. As the construction progresses, these arches are made longer and longer. The positioning of the blocks is maintained up to reaching the stairwell edge.

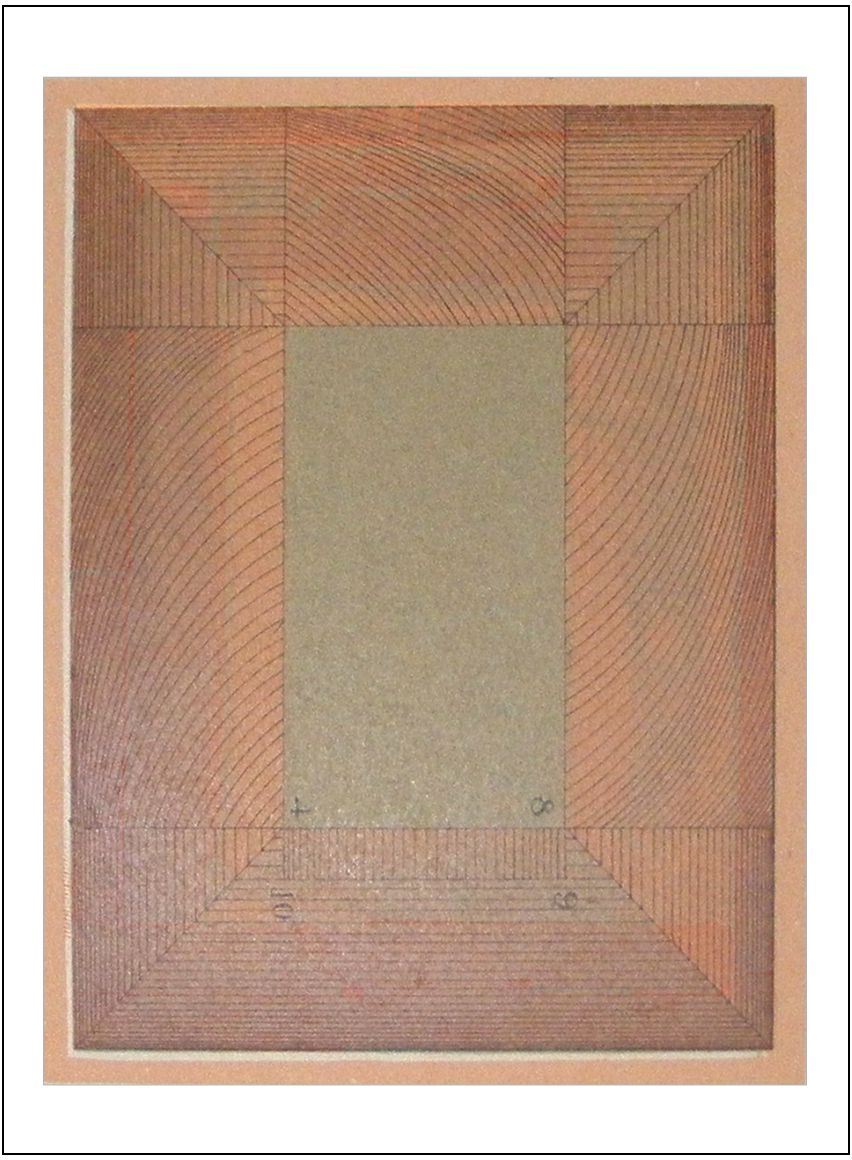

Fig. 6.5. Brick layout of a typical cantilevered stairway (Formenti 1893).

The lowest, skewed band of a flight is built first. Then the central band follows, built with bricks laid following the curve of the last course of the lowest band. The addition of the upper band concludes construction of the flight.

6.3 Other Types of Stairs

In some cases, the length of the stairhead does not allow for an open well. In such cases piers are constructed at the corners of the stairwell (fig. 6.6). In the case of stairways with a central spine wall, the flights are composed of long barrel vaults (fig. 6.7).

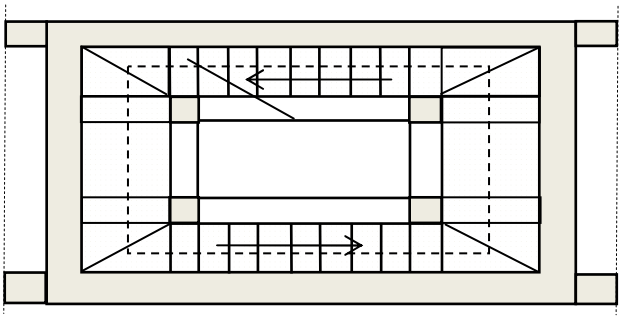

Fig. 6.6. Stairway with well on piers

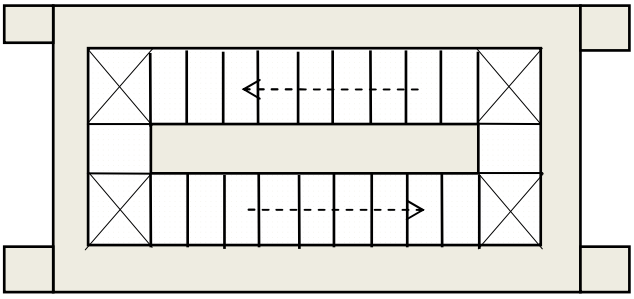

Fig. 6.7. Stairway with spine wall

6.4 Paradoxical Static Behavior of Cantilevered Masonry Stairs

To anyone used to working with the framework of reinforced concrete structures, cantilevered masonry stairways must give the impression of extreme static instability. In such a perspective, the existence of an admissible equilibrium may appear paradoxical. A widespread opinion holds that these structures are unsafe.

There are undoubtedly difficulties in formulating a consistent static model for these stairs taking into account the substantial incapacity of masonry to sustain tensile stresses. Their behavior has in fact long been the subject of in-depth study.

Figure 6.8 shows a photograph of a gypsum model of a cantilevered stairway under loading tests (Lenza 1983). As soon as the limit loads are exceeded, the first cracks occur transversely, at the middle of the free edge. Actually, it was expected that cracks would appear at the extrados, parallel to the axis of the flight, near the wall. No such cracks were however detected and the outcome is still a matter of debate (Baratta, 2007).

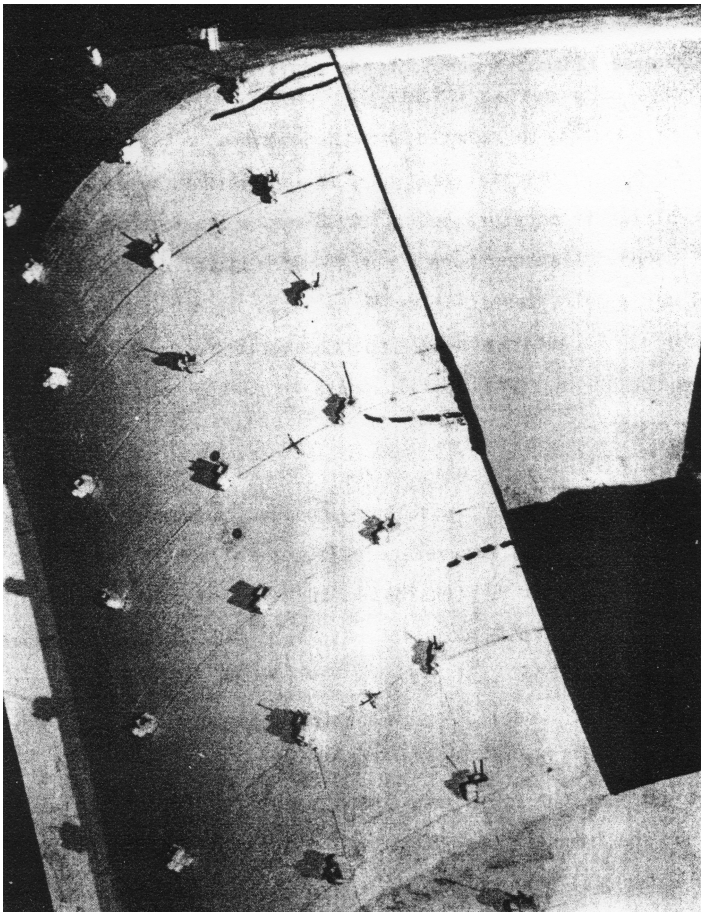

Fig. 6.8. Cracking pattern detected in the middle section of a gypsum model of a flight of stairs, by Lenza, (1983)

6.5 Numerical Investigations on the Statics of a Single Cantilevered Masonry Flight

Various working hypotheses can be formulated. In place of the cantilever model, in which loads transmission occurs through bending and shear in the transverse direction, we could instead imagine longitudinal loads transmission, able to mobilize longitudinal resistant arches. However, as can be easily appreciated, even if such systems could actually be achieved, they would transmit very high thrusts, generally incompatible with ordinary staircase geometries.

The weight of the flight must be sustained by the wall in which it is embedded. The contribution made by the intermediate landings, made up of thin cloister vaults, is in fact negligible with respect to that offered by the wall. So we can assume that the weight of the flight is conveyed wholly to the wall. By this simplifying assumption, the long vault is also subjected to torsional actions and the problem thus becomes understanding how transmission of such torsional loads can occur in the framework of no-tension behavior.

In this regard, one numerical investigation has been conducted (Soccolini, 2008 - 2009) using the nonlinear program ATENA (Cervenka, 2002) , which can take into account both the presence of very weak tensile strength as well as the occurrence of cracks. The numerical analyses were conducted first considering a long horizontal vault cantilevered from a side wall. The vault section is a quarter circle with end constraints unable to sustain vertical loads. Figure 6.9 shows a section of the vault inserted into the wall.

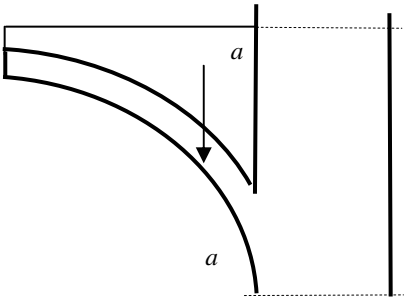

Fig. 6.9. Transverse vault section assumed in the first numerical study

The vault is 12 cm thick, with internal radius R =1 m. The length of the horizontal vault is 3 m. The loads per unit vault length, constant for the entire section, are:

masonry weight g_p=350 kg/m,

rubble weight g_r=860 kg/m,
live load: q=400 kg/m.

The $\sigma - \varepsilon$ equation is linear, with a tensile strength of 1 kg/cm^2 and a compression strength of 200 kg/cm^2.

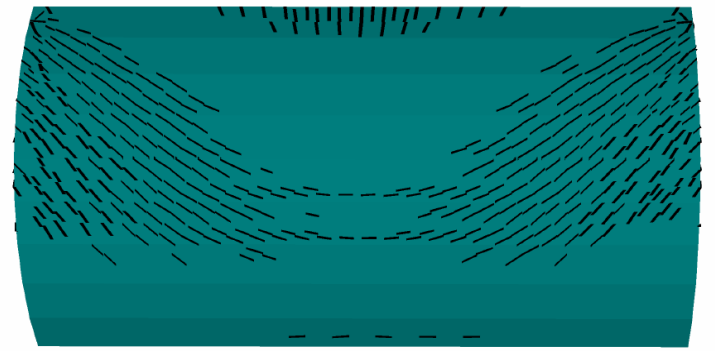

Fig. 6.10. Cracks at the extrados

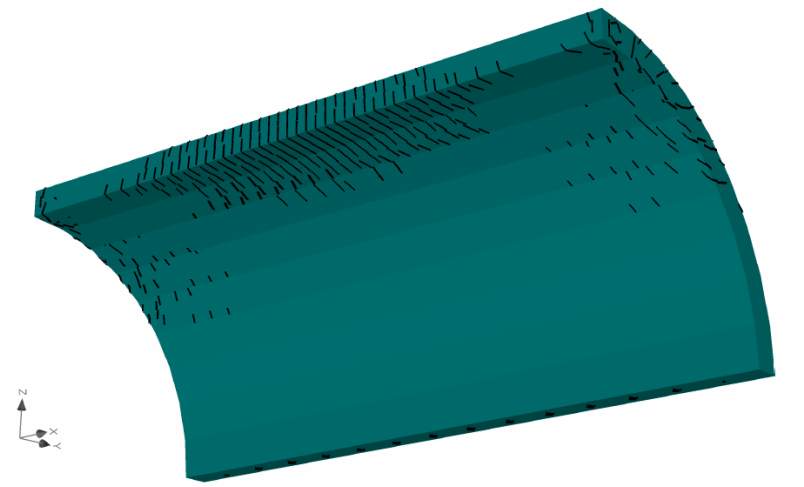

Fig. 6.11. Cracks at the intrados

The loads are applied gradually through 31 successive steps. Figures 6.10 and 6.11 show the resulting cracking patterns at the extrados and intrados of the vault, respectively. The cracks are very thin and for the most part indicate the direction of the compressions. Figures 6.12 and 6.13 show the principal directions of stress respectively on the extrados and intrados.

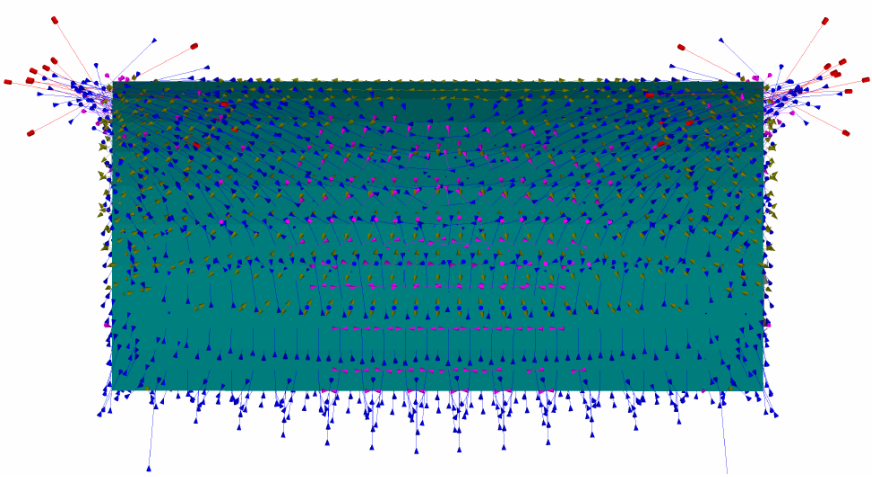

Fig. 6.12. Principal stress directions on the extrados

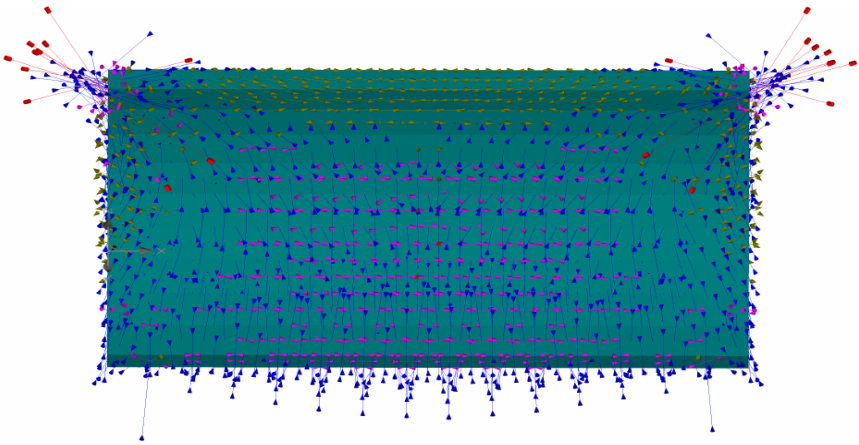

Fig. 6.13. Principal stress directions on the intrados

The resulting transverse cracks, vertically cutting the external longitudinal edge of the vault (Figs. 6.11 and 6.12), match the cracks detected by Lenza (1983) in the previously mentioned tests on a gypsum model of a flight of stairs (Fig. 6.8) The same analysis was then conducted on an inclined flight. The trials regarded a vertical stairway height of 1.70 m and a linear flight length of 30 m. Figure 6.14 shows the resulting cracking pattern on the extrados. Comparing this figure with the analogous Figure 6.11 for the horizontal vault shows that the crack patterns are

substantially similar, even if the influence of the inclination is noticeable. The results for the intrados cracking are the same.

Figures 6.13, 6.14, and 6.15 clearly reveal the occurrence of a longitudinal arching effect, with springings at the connection of the external vault edge with the landings. Thus, the loads are *conveyed transversely* to the wall along vertical half-arches compressed by the pushing action exerted by longitudinal arches.

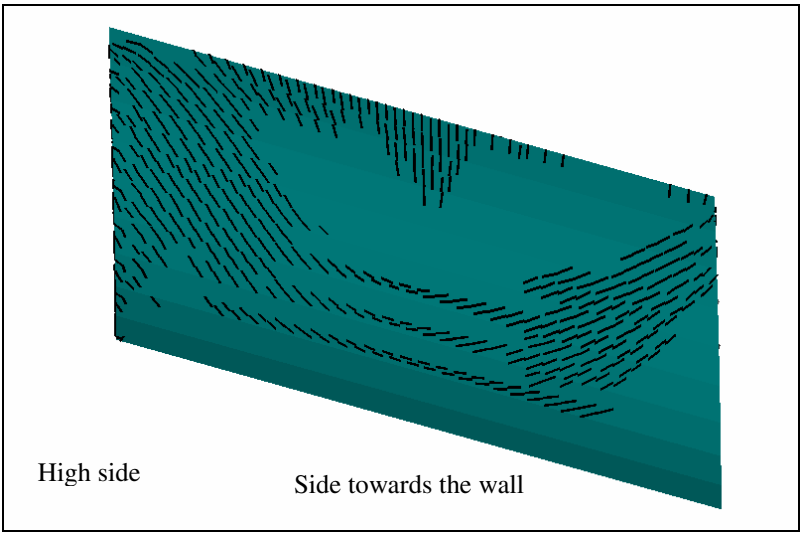

Fig. 6.14. The inclined flight. Cracks at the extrados

The cracking pattern confirms the occurrence of such longitudinal arching. The resulting cracking patterns are similar to those occurring on the intrados near the key section of a masonry arch under vertical loads. Comparing the cracking pattern on the intrados and the extrados in Figures 6.11 and 6.12 shows that the longitudinal arching arises mainly toward the vault extrados.

6.6 Resistant Model of a Horizontal Flight of Stairs with Side Landings

For the sake of simplicity, let us first examine the case of a vault with a horizontal axis. Any section of the the long vault is subjected to a *distributed torsional load*

$$m_T = \sum_i g_i x_i \,, \tag{1}$$

as shown in Fig. 6.15.

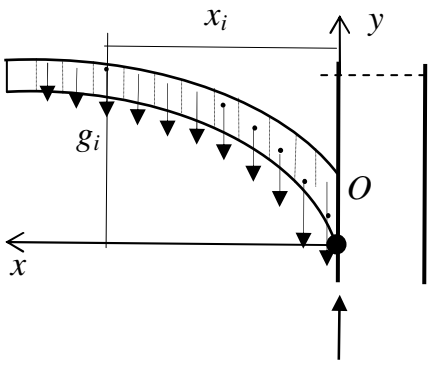

Fig. 6.15. Generation of the torsional load on the transversal vault sections

To sustain this action we can assume, according to the foregoing results, that the vault mobilizes a resistant system composed of (Fig. 6.16):

a) a series of *longitudinal flat arches,* contained within the vault along horizontal planes, which transmit their thrusts to the intersection of the flight's free edge with the landings;
b) a series of *transverse vertical half-arches* conveying the vertical loads to the longitudinal side wall.

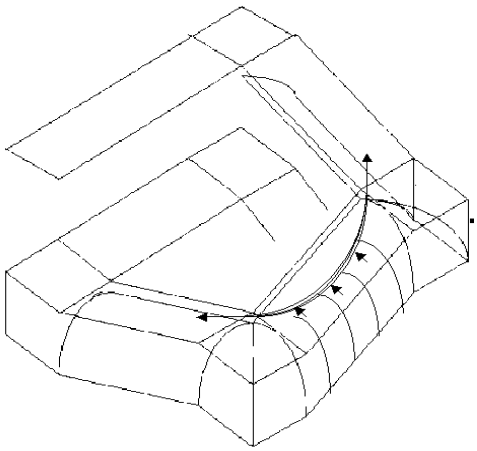

Fig. 6.16. Generation of the resistant system of a flight of stairs

The key point is the mobilization of compressions within these transverse half-arches, which enables them to transmit vertical loads. This compression is produced by the horizontal loads p_i conveyed by the longitudinal flat arches according to the scheme shown in Figures 6.16 and 6.17.

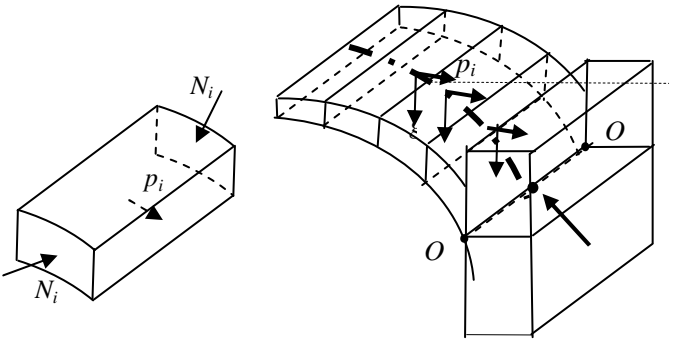

Fig. 6.17. Part of a flight subdivided into voussoirs, with the acting horizontal forces transmitted by the longitudinal arches and corresponding pressure line

We assume that each of these longitudinal arches is contained within a horizontal plane crossing the profile of the flight section and, for the sake of simplicity, that each is parabolic in profile, so that the horizontal load p_i is *constant* along the flight. In such a conception, the resistant system is able to absorb the torsion due to the misalignment between the resultant load g and the vertical wall reaction, which is assumed to pass though point O, the toe of the flight section (fig. 6.18). We will have

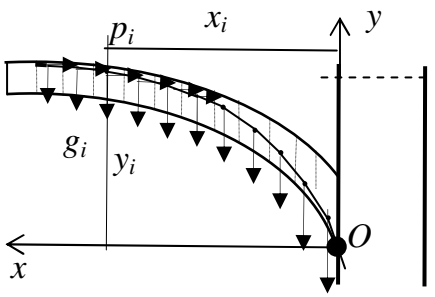

Fig. 6.18. The torsional equilibrium of the transversal vault sections

$$\sum_i g_i x_i = \sum_i p_i y_i \tag{2}$$

This condition will be satisfied by the distribution of loads p_i if the pressure line in the section profile passes through the toe O.

The key point here is thus the development of the longitudinal flat arches and, consequently, the horizontal forces p_i acting along the transverse half-arches.

The system constituted by a single cantilevered flight with the two side landings, fixed at rigid boundary walls, cannot become deformed by mechanisms. Masonry interpenetration is produced as soon as the loads are applied, so that only compression stresses can develop. Following up now on considerations advanced in Chapter II, we can affirm that any distribution of weights will produce conditions of admissible equilibrium in the system and that it will thus always be possible to specify a distribution of horizontal forces

$$p_i \tag{3}$$

which, together with the weights g_i, give rise to a transverse pressure line wholly contained within the section of the flight wall and passing through the toe O. All the weight g will be transmitted to the side and, consequently, the torsional equilibrium will be satisfied for every element of unit length of the vault section.

The flight pushes against its supports and a settlement will occurr. A slight enlargement of the span takes place accompanied by cracks occurring near the external edge at mid-sections of the flight and consequent cracks in the landings. A state of minimum thrust takes place in the horizontal flat arches and the research of the distribution of the loads p_i will be performed in order to minimize the thrust as it will be shown in the next sections.

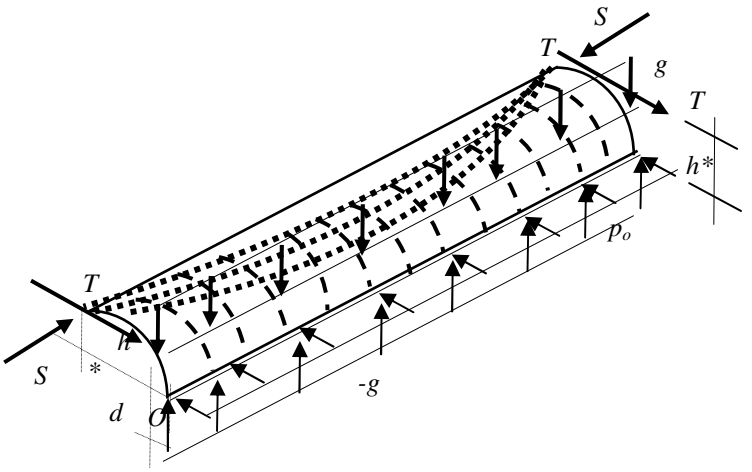

Fig. 6.19. Resistant system of a horizontal vault

Summing up all the loads p_i acting on the voussoirs constituting the vault, we obtain the horizontal load p_o representing the pushing load per unit length conveyed by the vault to the side wall:

$$p_o = \sum_i p_i \quad . \tag{4}$$

Uniform load p_o distributed along the length L of the vault is equilibrated by the two shears T, that is, the transverse components of the action transmitted by the vault to the side landings (fig.6.19)

$$p_o L = 2T \quad . \tag{5}$$

The shear T shown in Figure 6.18 is the component on the horizontal plane orthogonal to the flight edge of the overall force conveyed to the springing from all the longitudinal arches in the series. The two resultant shears T oppose the pushing load p_o exerted by the longitudinal wall. We can thereby obtain the arm h^* of the resisting global torque gLd (fig.6.19). For the global torsional equilibrium we thus obtain

$$gLd - 2Th^* = 0 \tag{6}$$

and

$$h^* = \frac{gLd}{2T} \quad . \tag{7}$$

For each load p_i there is one corresponding longitudinal arch of the series. The thrust S_i of these longitudinal arches applied at the intersection of the landing with the free side of the flight is

$$S_i = \frac{p_i L^2}{8 f_i} \quad , \tag{8}$$

where

$$f_i = f - x_i \tag{9}$$

is the corresponding sag of the arch. The overall thrust is

$$S = \sum S_i = \frac{L^2}{8} \sum \frac{p_i}{f - x_i} \quad . \tag{10}$$

The resulting internal stresses is both admissible and in equilibrium with the applied loads.

6.7 An Inclined Flight of Stairs

Let us now consider the case of a flight of stairs whose axis is inclined by an angle ϕ with respect to the horizontal (Fig. 6.20). The section of the flight is the same as in the previous case of a horizontal axis, as are the reference axes in the section. The overall torque is now lower, and is expressed by

$$M_T = g \cos\phi \cdot L \cdot d \tag{11}$$

Shears *T,* misaligned with the pushing load p_o, balance the torque (11) according to the relation

$$2Th^* \cos\phi = g \cos\phi Ld \quad . \tag{12}$$

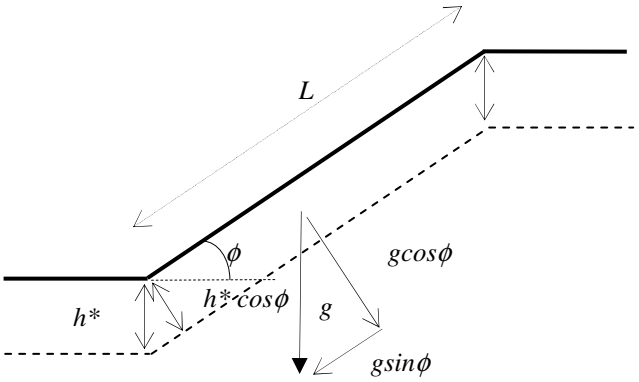

Fig. 6.20. Torsional load on an inclined flight

If the torque decreases, so does the arm of the resistant torque and

$$2Th^* = gLd \quad . \tag{13}$$

Both the pushing loads and the thrust transmitted by the series of horizontal arches to the side landings will have the same expressions (9) and (12) as for horizontal flights.

6.8 Determination of the Horizontal Forces p_i

The point of departure is to subdivide the section profile into a given number of voussoirs and then evaluate the corresponding weights g_i. The outer voussoir will be excluded because flat horizontal arches cannot form in the more external band.

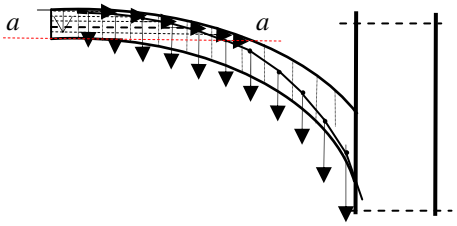

Fig. 6.21. Construction of the pressure curve within a transverse half-arch

It will be useful to trace the horizontal line *a* - *a* from the external corner of the intrados: this line borders the lower plane of the part of the section where the lowermost horizontal arch forms. Horizontal segments are then traced above this line to indicate other planes where horizontal arches form. Through trial and error, the horizontal forces p_i are found to be located mainly in the upper part of the profil *minimizing* the thrusts, as sketched out in Figure 6.21. A pressure line can be traced to remain as high as possible within the section and pass through point O. Forces p_i in the lower part of the section can generally be neglected and an iterative procedure can be applied.

6.9 Cantilevered Stairways as a Complex of Flights and Landings

By using the model of the single flight and two landings it is now possible to formulate the resistant model for the entire stairway. The play between the longitudinal flat arches and the transverse half-arches along two adjacent flights is shown in Figures 6.22 and 6.23. It should first be noted that the vertical components of the thrusts of a pair of adjacent flights mutually cancel.

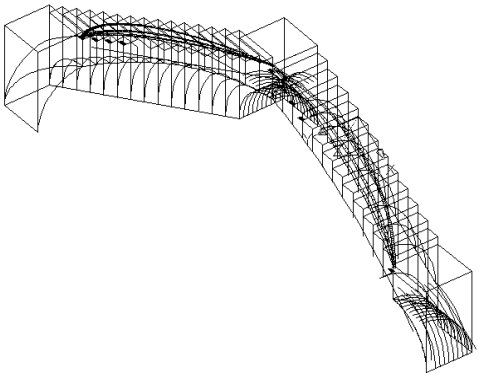

Fig. 6.22. Interplay between longitudinal and transverse half-arches of adjacent flights

In Figure 6.23, β is the angle formed by the inclined flight with respect to the horizontal, and subscripts u and l indicate quantities of the upper and lower flights, respectively. The actions conveyed to the horizontal edge of the landing, obtained by summing the thrust and the shear on the horizontal plane, are

$$(S_l \cos\beta - T_u) \qquad (S_u \cos\beta - T_l)\,. \tag{21}$$

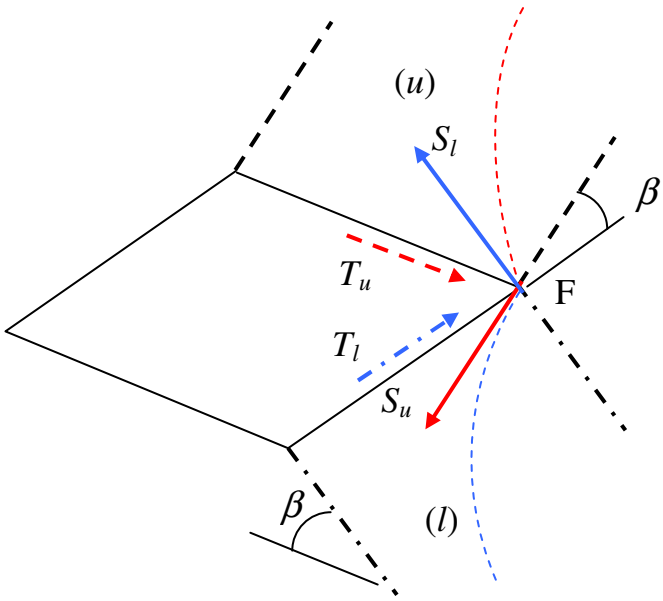

Fig. 6.23. Canceling of the vertical components of the actions conveyed by two adjacent flights (*s*) and (*i*). Indicated thrusts and shears are transmitted by landings.

When the flights are equal, we have

$$S_u = S_l = S, \qquad T_u = T_l = T\,. \tag{22}$$

In this case, the forces acting on each of the two edges of the landing are (Fig. 6.25)

$$(S\cos\beta - T)\,. \tag{23}$$

Figure 6.23 shows the plan of a staircase made up of four flights and four landings. For the sake of simplicity, the long stairhead has been omitted. The same figure shows the shear T and thrusts S acting at the *foci* of the stairs.

By considering the complex of the four flights, it can be seen that at each focus the sum of the shears T and the thrusts S yields a resultant acting along the horizontal diagonal of the landing constituted by one quarter of a thin cloister vault.

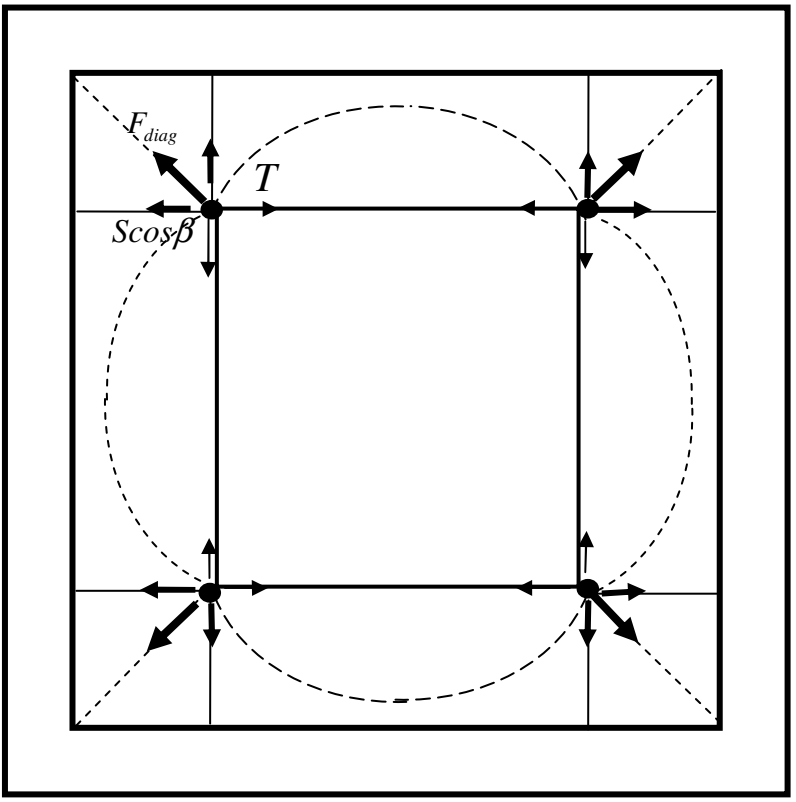

Fig. 6.24. Interactions between flights and actions on the external cage walls

The overall compression force acting on the vertex of the diagonal is thus

$$F_{diag} = \sqrt{2}(S\cos\beta - T) \ , \tag{24}$$

which, in turn, is conveyed to the corner of the staircase walls. This thrust is relatively moderate due to the contrasting effects of the thrust component, $S\cos\beta$, and the shear, T. Figure 6.24 shows an example evaluation of the actions on the cage walls by the flights of a typical staircase. We understand the importance of a solid stair cage, with walls of suitable thickness.

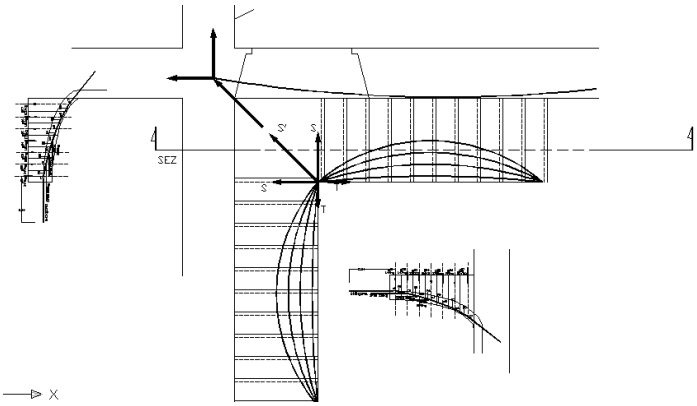

Fig. 6.25. Evaluation of thrust at staircase corners (Cartoni 2008 – 2009)

References

Baratta, A.: Sulla statica delle scale in muratura alla romana, Ingegneri Napoli, 6, Legoprint Campania, Napoli (2007)

Franco, G.: La scala tra valore simbolico e dimensione tecnica. Costruire in Laterizio (57) (1997)

Breymann, G.A.: Trattato generale di Costruzioni Civili, 1, Vallardi, Milan (1926)

Cervenka, V., Cervenka, J.: Atena program documentation, User's manual for Atena 2D, Prague (June 2002)

Di Luggo, A.: La scala nell'edilizia residenziale napoletanan. In: Applicazioni di Geometria Descrittiva e Rilievo Nell'Architettura " e-learning". Faculty of Architecture. University of Naples Federico II, Naples (2008)

Galiani, V. (ed.): Dizionario degli elementi costruttivi. UTET, Torino (2001)

Heyman, J.: The stone skeleton. In: Structural Engineering of Masonry Architecture. Cambridge University Press, Cambridge (1995)

D.M. (January 24, 1986)

Formenti, C.: La pratica del fabbricare, Atlante, vol. 2. Hoepli, Milan (1893)

Giovanetti, F. (ed.): Manuale del Recupero del Comune di Roma. DEI, Rome (1997)

Lenza, P.: Modelli di comportamento e direttrici di restauro delle scale in muratura realizzater con voltine a sbalzo. In: Quaderni di Teoria e Tecnica delle Strutture, Univ. di Napoili, Istit. Di Tecnica delle Coistruzioni, vol. (531) (1983)

Theses (University of Rome Tor Vergata, Rome, Italy)

Soccolini, N.: Ricerca di modelli resistenti delle rampe delle scale in muratura, supervisor, Como, M. (2008-2009)

Cartoni, D.: Sulla statica delle scale alla Romana, supervisor, Como, M. (2008-2009)